



LAWRENCE  
LIVERMORE  
NATIONAL  
LABORATORY

# A Reduced Mechanism for Biodiesel Surrogates for Compression Ignition Engine Applications

Z. Luo, M. Plomer, T. Lu, S. Som, D. E. Longman,  
S. M. Sarathy, W. J. Pitz

September 12, 2011

Fuel

## **Disclaimer**

---

This document was prepared as an account of work sponsored by an agency of the United States government. Neither the United States government nor Lawrence Livermore National Security, LLC, nor any of their employees makes any warranty, expressed or implied, or assumes any legal liability or responsibility for the accuracy, completeness, or usefulness of any information, apparatus, product, or process disclosed, or represents that its use would not infringe privately owned rights. Reference herein to any specific commercial product, process, or service by trade name, trademark, manufacturer, or otherwise does not necessarily constitute or imply its endorsement, recommendation, or favoring by the United States government or Lawrence Livermore National Security, LLC. The views and opinions of authors expressed herein do not necessarily state or reflect those of the United States government or Lawrence Livermore National Security, LLC, and shall not be used for advertising or product endorsement purposes.

## **A Reduced Mechanism for Biodiesel Surrogates for Compression Ignition Engine Applications**

Zhaoyu Luo<sup>a1</sup>, Max Plomer<sup>a</sup>, Tianfeng Lu<sup>a</sup>,

Sibendu Som<sup>b</sup>, Douglas E. Longman<sup>b</sup>

S.M. Sarathy<sup>c</sup>, William J. Pitz<sup>c</sup>

*<sup>a</sup>Department of Mechanical Engineering,  
University of Connecticut, Storrs, CT 06269-3139, USA*

*<sup>b</sup>Transportation Technology Research and Development Center,  
Argonne National Laboratory, Argonne, IL 60439, USA*

*<sup>c</sup>Physical and Life Sciences Directorate,  
Lawrence Livermore National Laboratory, Livermore, CA 94550, USA*

### **Abstract**

A skeletal mechanism with 89 species and 364 reactions for a tri-component biodiesel surrogate, which consists of methyl decanoate, methyl 9-decenoate and n-heptane, was developed to reduce computational costs for 3-D engine simulations. The detailed mechanism for biodiesel developed by Lawrence Livermore National Laboratory (LLNL) was employed as the starting mechanism. The rate constants for the n-heptane and larger alkane subcomponent in the detailed mechanism were first updated. The detailed mechanism was then reduced with direct relation graph (DRG), isomer lumping, and DRG-aided sensitivity analysis (DRGASA), which was improved to achieve a larger extent of reduction. The reduction was performed for pressures from 1 to

---

<sup>1</sup> Corresponding author.

Address: Department of Mechanical Engineering, University of Connecticut, 191 Auditorium Rd. Storrs, CT 06269-3139, USA. Tel.: +1 860 486 8465; fax: +1 860 486 5088

Email address: [luozy@engr.uconn.edu](mailto:luozy@engr.uconn.edu)

100atm and equivalence ratios from 0.5 to 2 for both extinction and ignition applications. The initial temperature for ignition was from 700-1800K, covering the compression ignition (CI) engine conditions. Extensive validations were performed against 0-D simulations with the detailed mechanism and experimental data for spatially homogeneous systems, 1-D flames and 3D-turbulent spray combustion. The skeletal mechanism was able to predict various combustion characteristics accurately such as ignition delay, flame lift-off length, and equivalence ratio at flame lift-off location under different ambient conditions. Compared with the detailed mechanism that consists of 3299 species and 10806 reactions, the skeletal mechanism features a reduction by a factor of 37 in size while still retaining good accuracy and comprehensiveness.

*Keywords: mechanism reduction; biodiesel; methyl decanoate; diesel engine; auto-ignition*

## 1. Introduction

Biodiesel is becoming one of the most promising renewable fuels as the global energy demand increases. Biodiesel can be used in existing diesel engines with reduced soot, CO, and unburned hydrocarbons (HC) emission without significant changes to their design [1]. The major component of biodiesel is fatty acid methyl esters (FAME), which feature the ester functional group and long carbon chains (e.g., C<sub>12</sub>-C<sub>18</sub>) with varying degrees of un-saturation. Due to the fuel's large molecular size and varying composition, the detailed chemical kinetics of biodiesel combustion is highly complex. Consequently, the detailed mechanisms for biodiesel are large in size [2-4]. For example, a recently published detailed mechanism for biodiesel surrogate consists of over 3000 species and 10000 reactions [3]. 3-D engine simulations with such large mechanisms are infeasible, particularly when attempting to characterize low temperature and negative temperature coefficient (NTC) reactivity. However, since computational modeling drives the design of engines and combustors, accurate prediction of fuel combustion and pollutant emissions requires comprehensive chemical kinetics. Reduction of the large mechanisms is therefore necessary to accommodate realistic chemistry in practical engine simulations.

Mechanism reduction has been extensively studied over the last few decades, as reviewed in Ref. [5]. One of the major classes of reduction methods is skeletal reduction, which eliminates unimportant species and reactions from detailed mechanisms using such methods based on sensitivity analysis [6-7], principle component analysis [8-9], Jacobian analysis and computational singular perturbation [10-12], directed relation graph (DRG) [13] and other DRG-based methods [14-15]. In particular, the DRG method was based on reaction rate and species flux analyses, and does not involve Jacobian matrix evaluation and factorization. Therefore, it

features low reduction cost compared to most other reduction methods. DRG was recently extended to DRG-X by Lu et al. [16]. By accommodating expert knowledge on chemical kinetics into mechanism reduction, DRG-X was able to develop skeletal mechanisms with higher accuracy compared to the original DRG method. DRG-based methods can be combined with sensitivity analysis to further reduce the skeletal mechanisms, e.g. through DRG-aided sensitivity analysis (DRGASA) [17-18] and DRGEP with sensitivity analysis (DRGEPSA) [19].

After the skeletal reduction, other methods can be further applied on the skeletal mechanisms to further reduce the size of the mechanism, e.g., through lumping methods [20-24] that group the correlated species. In particular, isomer lumping [25-26] can be employed to group the isomers in mechanisms for large hydrocarbons that feature nearly-identical thermo and transport properties. It is noted however that, although there have been a large number of methods developed for mechanism reduction, reduced mechanisms for biodiesel that are suitable for 3-D engine simulations are rare, particular when low temperature chemistry is involved. This is primarily because of the large size of biodiesel mechanisms and consequently the difficulties in the reduction itself. In previous works, a reduced mechanism with low-temperature chemistry for methyl butanoate (MB) was developed by Brakora et al., and validated under biodiesel-fueled engine conditions [27]. The reduced mechanism consists of 41 species and 150 reactions, which is small enough for 3-D engine simulations. However, the chain length of MB is short compared with that of real biodiesel. Hence it is inadequate to accurately represent the physicochemical properties of biodiesel. Moreover, it is observed in experimental and kinetic studies that MB does not adequately characterize the NTC behavior of large hydrocarbons [28], and its mechanism cannot accurately predict the flame lift-off and emission characteristics of biodiesel combustion [29].

Methyl decanoate (MD) was later recognized as a more viable surrogate to biodiesel fuels since it features both a long carbon chain as well as the ester group. A comprehensive and accurate skeletal mechanism for MD with low temperature chemistry was derived using DRG for 1-D flame analysis by Sarathy et al. [30]. However, this skeletal mechanism consists of more than 600 species thus is not suitable for 3-D engine simulations. Skeletal mechanisms for the biodiesel surrogate were then developed using DRG-based methods and lumping [31-33]. The surrogate mixture consists of MD, methyl-9-decanoate (MD9D) and n-heptane, which can better represent the physical properties and combustion features of biodiesel [3]. The skeletal mechanism in Ref. [32] consists of 118 species and 837 reactions. It however doesn't consist of the low temperature chemistry thus is not suitable for CI engine applications. Another skeletal mechanism that can be applied in engine simulations was developed by Brakora et al. [33]. It features small mechanism size of 77 species and 216 reactions with low temperature chemistry, but has been tuned to match only certain experimental conditions.

In the present study, the n-heptane and larger alkane subcomponent in the detailed mechanism for biodiesel from LLNL is first updated for improved prediction of the NTC behavior. The updated mechanism is then employed as the starting mechanism for the reduction. An integrated reduction method that combines DRG, isomer lumping, and DRGASA is applied for the reduction. The method of DRGASA is improved to achieve a higher extent of reduction, such that smaller skeletal mechanisms can be obtained for more efficient multi-dimensional engine simulations. Extensive validations against spatially homogeneous system, 1-D flames and 3-D engine experiments are further performed to show the high chemical fidelity of the resulting skeletal mechanism.

## 2. Methodologies

### 2.1 Update of the detailed mechanism

The detailed mechanism used in the present reduction was originally developed by Lawrence Livermore National Laboratory (LLNL). The mechanism is for biodiesel surrogate mixtures of MD, MD9D and n-heptane, and consists of 3299 and 10806 elementary reactions. The tri-component surrogate mixture allows the flexibility in matching the physical and important combustion properties of real biodiesel from different feed-stocks. For example, the ignition delay times can be fine tuned by varying the composition of the surrogate mixture to match the data of the real fuel.

Prior to reduction, several updates were made to the detailed mechanism to make it consistent with rate rules present in current LLNL n-heptane and larger alkane mechanisms [34-35]. The following is a summary of the changes made to the detailed mechanism:

- The uni-molecular decomposition reactions of n-heptane and the beta-decomposition reactions of heptyl radicals were replaced by those in LLNL's most recent n-heptane mechanism [34].
- The reaction rate constants for alkyl peroxy radical isomerizations (i.e.,  $RO_2=QOOH$ ) and carbonyl-hydroperoxide formation (i.e.,  $O_2QOOH=carbonyl-hydroperoxide + OH$ ) for n-heptane, MD, and MD9D related species were made consistent with the latest large alkane reaction rate rules [34-35]. Specifically, the activation energies for these reactions were reduced by 400 cal/mol to increase the low temperature reactivity.
- The reaction rate constants for carbonyl-hydroperoxide decomposition for n-heptane, MD, and MD9D related species were made consistent with Refs. [34-35]. The activation energy

for these reactions was decreased to 39,000 cal/mol to better predict low temperature ignition delay times for n-alkanes [34-35].

## **2.2 Mechanism reduction**

Following the above modifications, the reduction of the detailed mechanism was performed based on a large set of reaction states sampled within the parameter space of pressures from 1 to 100atm, equivalence ratios from 0.5 to 2.0, initial temperatures from 700 to 1800K for auto-ignition, and inlet temperature of 300K for extinction in perfectly stirred reactors (PSR). Note that the NTC region which is important for auto-ignition under CI engine conditions was covered in the reduction. Jet stirred reactors (JSR) with diluted mixtures and intermediate temperatures were also included in the sampling. The fuel mixture consists of 25% MD, 25% MD9D and 50% n-heptane in mole. The worst case error tolerance was set to be 30%. Such an error tolerance is comparable to the overall uncertainty of the detailed mechanism, as such there is no significant loss in chemical fidelity through the skeletal reduction [32]. It will be further shown in the next section that the resulting skeletal mechanism obtained with such an error tolerance performs well in predicting experimental data in most cases compared with the detailed mechanism.

The method of DRG [32] was first applied to eliminate unimportant species and reactions from the detailed mechanism, and a 664-species skeletal mechanism was obtained. Isomer lumping [25] was subsequently applied to the 664-species skeletal mechanism to group the isomers with similar thermo and transport properties to further reduce the mechanism size, resulting in a 641-species skeletal mechanism. To overcome the challenge to further reduce the mechanism to less than about 100 species, a revised DRGASA method was employed in the present reduction. Based on the previous procedure in Refs. [17-18], the reduction error induced

by eliminating a species is first estimated in DRGASA, such that the errors can be sorted in ascending order for sequential sensitivity analysis of species elimination. Previous studies with DRGASA excluded important species with estimated errors larger than, say, 50% from the global sensitivity analysis, because they may cause difficulties in convergence and subsequently long computation time if they are selected for elimination by the DRGASA algorithm. However, the primary concern in the present work is the final size of the mechanism, rather than the reduction cost. Therefore, almost every species was included in the global sensitivity analysis to ensure that the resulting mechanism is minimal in size. A 140-species mechanism was consequently obtained with increased reduction cost.

To achieve a larger extent of reduction, error cancellation was further utilized in the revised DRGASA to minimize the mechanism size in the present work. The effect of error cancellation for mechanism reduction is demonstrated in Fig. 1 with two species A and B. It is seen that removing either A or B individually from the detailed mechanism results in errors with opposite signs, while removing A and B together results in a skeletal mechanism with a smaller error compared to those by eliminating A and B individually. In the present reduction, if the individual eliminations of two species result in opposite errors, sensitivity analysis will be performed by test-eliminating the pair of species together. If the error induced by the test-elimination is smaller than the error tolerance, the elimination will be committed. This process is repeated until no individual species or species pairs can be further eliminated based on the given error tolerance. It is noted that only species with small individual errors, e.g. smaller than 40%, were considered for error cancellation to avoid substantial reduction in the chemical fidelity of the final mechanism. Using the revised DRGASA, a skeletal mechanism with 89 species and 364 elementary reactions was eventually obtained.

### 2.3 Simulations of 3-D Turbulent Spray Combustion

The 89-species skeletal mechanism was then used in 3-D spray-combustion simulations for validation, in addition to the 0-D and 1-D simulations. The 3-D simulations were performed using the Eulerian-Lagrangian approach in the computational fluid dynamics (CFD) software CONVERGE [36-38]. It incorporates state-of-the-art models for spray injection, atomization and breakup, turbulence, droplet collision, and coalescence. The gas-phase flow field is described using the Favre-Averaged Navier-Stokes equations in conjunction with the RNG k- $\epsilon$  turbulence model, which includes source terms for the effects of dispersed phase on gas-phase turbulence. These equations are solved using a finite volume solver. The details of these models can be found in previous publications [29, 39-40], hence only a brief description is provided here.

Fuel injection is simulated using the blob injection model. Following the injection, Kelvin Helmholtz (KH) and Rayleigh Taylor (RT) models are used to predict the primary and secondary breakup of the computational parcels [41-42]. A breakup length is used within which the KH model is used to predict the primary breakup. Beyond the breakup length, the KH and RT models compete in breaking up the droplets. Droplet collisions are based on the no time counter algorithm [43]. Once collision occurs, the outcomes of the collision are predicted as bouncing, stretching, reflexively separating, or coalescing [44]. A droplet evaporation model based on the Frossling correlation [38] is used in the present simulations. A dynamic drag model is also used postulating that the drag coefficient depends upon the shape of the droplet, which can vary between a sphere and a disk [45]. The effects of turbulence on the droplet are also included, using a stochastic turbulent dispersion model. Kinetic modeling in CONVERGE is performed using the SAGE chemical kinetic solver [36], and is directly coupled with the gas-phase calculations using a well-stirred reactor model. The soot mass production within a

computation cell is determined from a single-step competition between formation and oxidation rates of  $C_2H_2$  species based on the Hiroyasu model [38], which has been extensively used in engine-modeling literature.

CONVERGE uses an innovative, modified cut-cell Cartesian method for grid generation. The grid is generated internally to the code at runtime. For all cases, the base grid size was fixed at 4 mm. In order to resolve the flow near the injector, a fixed grid embedding is employed such that the minimum grid size is 0.25 mm. Apart from this region, it is rather difficult to determine *a priori* where a refined grid is needed. Hence, four levels of adaptive mesh refinement are employed for the velocity field. In order to match the combustion chamber geometry used in the experimental study [46], a cubical geometry of 108 mm on each side is generated (cf. Fig. 2). The zoomed-in view of the fixed embedding region is also shown. The temperature-dependent fuel properties of soy biodiesel, such as density, kinematic viscosity, surface tension, vapor pressure, heat of vaporization, and specific heat, were obtained from Ra et al. [47].

### **3. Results and discussion**

#### **3.1 Mechanism validation**

The 89-species skeletal mechanism for biodiesel surrogate was first validated against the detailed mechanism in homogeneous applications including auto-ignition and PSR. Figure 3a shows the ignition delay time as a function of the initial temperature calculated using the detailed and skeletal mechanisms for different equivalence ratios and initial temperatures covered in the reduction process. In general, good accuracy was observed. Figure 3b compares the temperature profiles of PSR calculated using the skeletal mechanism to that using the detailed mechanism, at various equivalence ratios and pressures. It is seen that the skeletal mechanism accurately

mimics the branches above the upper turning points, which are known as the extinction states. Some larger discrepancies were observed on the middle branches of the curves. This is due to the fact that those reaction states are not relevant to stable combustion systems at steady state. Hence, the reaction states on the middle branches were not included in the sample space for the present reduction.

### **3.2 Extended validations with 0-D and 1-D experiments**

The updated detailed mechanism and the 89-species skeletal mechanism were then validated against the experimental measurements for homogenous applications including auto-ignition and JSR. In the present study, the same fuel mixture as that in the reduction process, i.e. 25% MD, 25% MD9D and 50% n-heptane in mole, is used in the simulations. Figure 4 compares the calculated ignition delay time for n-heptane-air mixture with the experiments at various initial temperatures under fuel lean condition ( $\phi = 0.4$ ). The experimental data were reported by Herzler et al. [48]. It can be observed in Fig.4 that both mechanisms predict the experimental trends of ignition delay fairly well. In addition, the 89-species skeletal mechanism shows better agreement with the experimental results at low-temperature conditions. Figure 5 shows the comparison between the calculated and measured ignition delay times for a MD-oxygen-argon mixture. The experimental data was obtained from Ref. [49]. It is seen that the simulations with both mechanisms agree well in trend with the experiments, while the skeletal mechanism again agrees better with the experimental data. The skeletal and detailed mechanisms were further compared with the experimental measurements for the oxidation of rape-seed methyl ester (RME) in JSR. The experimental study was reported by Dagaut et al. [50]. Figure 6 compares the calculated species profiles for the biodiesel surrogate mixture with the experimental results at

various equivalence ratios in JSR with nitrogen dilution. Fair agreement was again observed, while the skeletal mechanism shows a better prediction than the detailed mechanism for certain species, e.g.  $C_2H_4$ .

Next, the skeletal mechanism is validated for 1-D flames, including both premixed and non-premixed flames. Since it is difficult to simulate the 1-D flames using the large detailed mechanism, only the results from the skeletal mechanism are shown in Fig. 7, where the experimental data for the premixed flame speed was taken from Ref. [51] for MD-air mixtures under atmospheric pressure. A worst case discrepancy of about 10cm/s is observed at fuel-rich conditions. Figure 8 plots the calculated temperature and species profiles with the skeletal mechanism along with the measured data by Sarathy et al. [52] for a non-premixed counter-flow flame of MD at atmospheric pressure. The diluted MD (1.8%MD and 98.2% $N_2$  in mole) mixture was used as the fuel in the simulation to match the experimental condition. In addition, the same boundary conditions from the experimental configuration were used for inlet temperatures, mixture compositions, and flow velocities. The predictions of temperature and species profiles are overall encouraging. In particular, the calculated major species profiles for MD, CO, and  $CO_2$  are in excellent agreement with the experimental data. The above validations therefore indicate that the 89-species skeletal mechanism can well capture the biodiesel combustion characteristics in both homogeneous and diffusive systems.

### **3.3 3-D simulations at CI engine conditions**

Further validation of the 89-species biodiesel surrogate mechanism is performed in a 3-D constant volume combustion chamber under CI engine conditions [53-55]. The experiments were performed by Nerva et al [56]. with the experimental conditions listed in Table 1. Validations

under non-reacting conditions are first presented followed by those under reacting conditions. Since liquid penetration, vapor penetration, lift-off length, and ignition delay data will be used for validation of the mechanism, these parameters will be first defined here. In simulations, liquid penetration is defined as the axial location encompassing 97% of the injected mass at that instant of time. Vapor penetration at any time is determined from the farthest downstream location of 0.05% fuel mass-fraction contour. Similarly, flame lift-off length is also calculated based on the mass fraction calculation of OH radical and is determined by the nearest upstream location of  $Y_{OH}=0.05\%$  contour. Ignition delay is defined as the time from start of injection to the time when temperatures above 2000K are first observed in any computational cell.

Figure 9 presents predicted and measured liquid spray and fuel vapor penetration at different times after the start of injection (ASI) at an ambient temperature of 900K. Spray penetration initially increases with time and then stabilizes at a quasi-steady value, which is called the liquid length. Hence, beyond this axial distance, liquid fuel is absent. The fuel vapor penetration though increases with time and is instrumental in fuel-ambient air mixing. It is seen that the simulations are able to capture the liquid spray and vapor penetration characteristics very well.

Following the validations under non-reacting conditions, Figs. 10-13 show the validations under reacting conditions. Figure 10 first compares the measured and computed OH profiles under conditions presented in Table 1 at ambient temperatures of 900K and 1000K. Due to the axi-symmetric nature of the spray and combustion processes, images are presented on a cut-plane through the center of the fuel jet. The flame lift-off location is shown by the red dashed line and the average equivalence ratio at flame lift-off location is also shown. The spray axis is demarcated using a white dashed line. The field of view is 75 mm x 25 mm in the axial and

radial directions respectively. The width and length of the flame is well captured by the simulations at both ambient temperature conditions.

The lift-off length is observed to be marginally over-predicted by the simulations under both ambient temperature conditions. Since lift-off length is over-predicted, it is not surprising that the average equivalence ratio at lift-off is marginally under-predicted by the simulations. For example, a calculated equivalence ratio of 2.04 compares fairly well to the experimentally measured value of 2.08 at 1000K. It is noted that the definitions used for calculating equivalence ratio values at the lift-off locations are different between experiments and simulations. Equivalence ratio is not a direct measurement from experiments, therefore flame lift-off length values are used in the analytical expressions by Naber and Siebers [57] to obtain the average equivalence ratios. In the present simulations, equivalence ratio is averaged over a transverse line 8mm long at the lift-off location (as shown in Fig. 10). The dimension of the transverse line depends upon the width of the flame and is selected to ensure that the significant temperature and equivalence ratio gradients are encompassed. Considering the difference in definitions of equivalence ratio values, the proximity of simulation and experimental values is very encouraging.

The lift-off length, ignition delay, and equivalence at lift-off length values are further summarized in Table 2. The ignition delay is over-predicted at 900K by the simulation with the calculated value being 0.741 ms versus a measured value of 0.683 ms. However, at 1000K ambient temperature condition, the ignition delay is marginally under-predicted with the calculated value being 0.391 ms versus a measured value of 0.396 ms. Since it has been observed in Fig.9 that the model predicted the mixing process quite well, the differences in flame lift-off

length and ignition delay in the present study could be primarily due to either the uncertainties in the detailed mechanism or the reduction error in the skeletal mechanism.

Figures 11 and 12 present the validations of simulated OH and soot contours against the chemiluminescence and Laser Induced Incandescence (LII) data, respectively, at different time during the combustion event at an ambient temperature of 1000K. It is seen in Figs. 11 and 12 that the experimental OH and soot contours are well predicted by the simulations in terms of location and occurrence during the combustion event. In addition, the shape in terms of width and length of OH and soot mass fraction contours were well predicted by the simulations. It is noted that although there are differences in ignition delay and lift-off length predictions (cf. Table 2 and Fig. 10), OH and soot contours were well captured by the models.

Figure 13 presents measured soot volume fraction and predicted soot mass fraction results at 3000  $\mu$ s ASI for both ambient temperature conditions. The corresponding lift-off length location is also represented by the dashed lines. It is noted that soot volume fraction distribution could not be obtained from simulations because the density of soot particles is not known. Also, since  $C_2H_2$  was used as a precursor for soot formation, the simulation results only aim to capture qualitative trends of soot production for biodiesel at different ambient temperatures. At both ambient temperature conditions the location of soot formation and soot distribution is well predicted by the simulations. In addition, the simulations were also able to capture the fact that the soot prediction decreases with the decrease in ambient temperature. Considering the fact that the detailed and the skeletal mechanisms were not tuned for the experimental conditions, such small discrepancy between predictions and experimental data is quite encouraging. Future studies will involve testing the 89 species mechanism against experimental data from CI engines

running on soy biodiesel. It is also noted that a quantitative prediction of soot distribution could be obtained by implementing the soot modeling approach of Vishwanathan and Reitz [58].

#### **4. Concluding Remarks**

An 89-species skeletal mechanism for biodiesel surrogate (MD, MD9D and n-heptane) including low-temperature chemistry was developed with DRG-based methods. The rate constants for the n-heptane and larger alkane subcomponent in the detailed mechanism developed by LLNL were first updated to be consistent with rate rules present in the current LLNL n-heptane and larger alkane mechanisms. The updated detailed mechanism was validated with experimental data including the ignition delays of n-heptane and MD, and the species profiles of MD in JSR.

The updated detailed mechanism was then reduced by subsequently applying DRG, isomer lumping and DRGASA. Substantial reduction in the mechanism size was achieved by carefully utilizing error cancellation in the reduction by DRGASA. In the present study, only the species with errors smaller than 40% were considered in error cancellation. Comprehensive validations of the skeletal mechanism against the detailed mechanism were further carried out to guarantee its chemical fidelity. The validations show that the small skeletal mechanism performs well over a wide range of parameters for both ignition and extinction applications. Nevertheless, it is worth noting that although larger extents of reduction can be achieved by utilizing error cancellation, the chemical fidelity of the resulting mechanism may not be guaranteed, particularly in predicting the concentrations of the intermediate species. This point is similar to the original DRGASA method. Therefore, the skeletal mechanisms developed using DRGASA

with or without error cancellation should be carefully validated before being applied in combustion simulations.

Extended validations were further performed for various experimental conditions including homogenous system, 1-D flames and 3-D turbulent spray combustion at CI engine conditions. The mechanism is shown to be versatile and robust since it performs satisfactorily in predicting the ignition delay and flame lift-off length, as well as the OH and soot concentration profiles under a variety of conditions. As such the 89-species skeletal mechanism is suitable for multi-dimensional engine combustion simulations with biodiesel fuels.

### **Acknowledgements**

The work at University of Connecticut was supported by the National Science Foundation under Grant 0904771. Any opinions, findings, and conclusions or recommendations expressed in this material are those of the authors and do not necessarily reflect the views of the National Science Foundation.

The submitted manuscript has been created by UChicago Argonne, LLC, operator of Argonne National Laboratory (Argonne). Argonne, a U.S. Department of Energy Office of Science laboratory, is operated under Contract No. DE-AC02-06CH11357. The U.S. Government retains for itself, and others acting on its behalf, a paid-up, nonexclusive, irrevocable worldwide license in said article to reproduce, prepare derivative works, distribute copies to the public, and perform publicly and display publicly, by or on behalf of the Government.

The work at LLNL work was supported by the US Department of Energy, Office of Vehicle Technologies, and the authors thank program managers Gurpreet Singh and Kevin Stork. This work was performed under the auspices of the US Department of Energy by Lawrence Livermore National Laboratory under Contract DE-AC52-07NA27344.

The authors thank Dr. Lyle Pickett from Sandia National Laboratories for sharing the flame lift-off data and many insightful discussions.

### References

- [1] A. Deepak, S. Sinha, K.A. Agarwal, Experimental investigation of control of NO<sub>x</sub> emissions in biodiesel-fueled compression ignition engine, *Renewable Energy*, **31** (2006) pp.2356-2369.
- [2] O. Herbinet, W. J. Pitz, C.K. Westbrook, Detailed chemical kinetic oxidation mechanism for a biodiesel surrogate, *Combust. Flame*, **154** (2008) pp.507-528.
- [3] O. Herbinet, W.J. Pitz, C.K. Westbrook, Detailed chemical kinetic mechanism for the oxidation of biodiesel fuels blend surrogate, *Combust. Flame*, **157** (2010) pp.893-908.
- [4] C.K. Westbrook, C.V. Naik, O. Herbinet, W.J. Pitz, M. Mehl, S.M. Sarathy, H.J. Curran, Detailed chemical kinetic reaction mechanisms for soy and rapeseed biodiesel fuels, *Combust. Flame*, **158** (2011) pp.742-755.
- [5] T.F. Lu, C.K. Law, Toward accommodating realistic fuel chemistry in large-scale computations, *Prog. Energy Combust. Sci.*, **35** (2009) pp.192-215.
- [6] A.S. Tomlin, M.J. Pilling, T. Turanyi, J.H. Merkin, J. Brindley, Mechanism reduction for the oscillatory oxidation of hydrogen - sensitivity and quasi-steady-state analyses, *Combust. Flame*, **91** (1992) pp.107-130.
- [7] T. Turanyi, Sensitivity analysis of complex kinetic systems - tools and applications, *J. Math. Chem.*, **5** (1990) pp.203-248.
- [8] S. Vajda, P. Valko, T. Turanyi, Principal component analysis of kinetic-models, *Int. J. Chem. Kinet.*, **17** (1985) pp.55-81.
- [9] S. Vajda, T. Turanyi, Principal component analysis for reducing the Edelson-Field-Noyes model of the Belousov-Zhabotinsky reaction, *J. Phys. Chem.*, **90** (1986) pp.1664-1670.
- [10] T. Turanyi, Reduction of large reaction-mechanisms, *New J. Chem.*, **14** (1990) pp.795-803.
- [11] A. Massias, D. Diamantis, E. Mastorakos, D.A. Goussis, An algorithm for the construction of global reduced mechanisms with CSP data, *Combust. Flame*, **117** (1999) pp.685-708.
- [12] M. Valorani, F. Creta, D.A. Goussis, J.C. Lee, H.N. Najm, An automatic procedure for the simplification of chemical kinetic mechanisms based on CSP, *Combust. Flame*, **146** (2006) pp.29-51.
- [13] T.F. Lu, C.K. Law, A directed relation graph method for mechanism reduction, *Proc. Combust. Inst.*, **30** (2005) pp.1333-1341.
- [14] P. Pepiot-Desjardins, H. Pitsch, An efficient error-propagation-based reduction method for large chemical kinetic mechanisms, *Combust. Flame*, **154** (2008) pp.67-81.

- [15] W. Sun, Z. Chen, X. Gou, Y. Ju, A path flux analysis method for the reduction of detailed chemical kinetic mechanisms, *Combust. Flame*, **157** (2010) pp.1298–1307.
- [16] T. Lu, P. Max, Z. Luo, S.M. Sarathy, W.J. Pitz, S. Som, D.E. Longman, Directed relation graph with expert knowledge for skeletal mechanism reduction. 7th US National Combustion Meeting, Atlanta, GA, 2011.
- [17] R. Sankaran, E.R. Hawkes, J.H. Chen, T. Lu, C.K. Law, Structure of a spatially developing turbulent lean methane-air Bunsen flame, *Proc. Combust. Inst.*, **31** (2007) pp.1291-1298.
- [18] X.L. Zheng, T.F. Lu, C.K. Law, Experimental counterflow ignition temperatures and reaction mechanisms of 1,3-butadiene, *Proc. Combust. Inst.*, **31** (2007) pp.367-375.
- [19] K. Niemeyer, C. Sung, M. Raju, Skeletal mechanism generation for surrogate fuels using directed relation graph with error propagation and sensitivity analysis, *Combust. Flame*, **157** (2010) pp.1760-1770.
- [20] S.S. Ahmed, F. Mauss, G. Moreac, T. Zeuch, A comprehensive and compact n-heptane oxidation model derived using chemical lumping, *Phys. Chem. Chem. Phys.*, **9** (2007) pp.1107-1126.
- [21] G.Y. Li, A.S. Tomlin, H. Rabitz, J. Toth, A general-analysis of approximate nonlinear lumping in chemical-kinetics .1. Unconstrained lumping, *J. Chem. Phys.*, **101** (1994) pp.1172-1187.
- [22] G.Y. Li, H. Rabitz, J. Toth, A general-analysis of exact nonlinear lumping in chemical-kinetics, *Chem. Eng. Sci.*, **49** (1994) pp.343-361.
- [23] A.S. Tomlin, G.Y. Li, H. Rabitz, J. Toth, A general-analysis of approximate nonlinear lumping in chemical-kinetics .2. Constrained lumping, *J. Chem. Phys.*, **101** (1994) pp.1188-1201.
- [24] E. Ranzi, M. Dente, A. Goldaniga, G. Bozzano, T. Faravelli, Lumping procedures in detailed kinetic modeling of gasification, pyrolysis, partial oxidation and combustion of hydrocarbon mixtures, *Prog. Energy Combust. Sci.*, **27** (2001) pp.99-139.
- [25] T.F. Lu, C.K. Law, Strategies for mechanism reduction for large hydrocarbons: n-heptane, *Combust. Flame*, **154** (2008) pp.153-163.
- [26] P. Pepiot-Desjardins, H. Pitsch, An automatic chemical lumping method for the reduction of large chemical kinetic mechanisms *Combust. Theory Model.*, **12** (2008) pp.1089-1108.
- [27] J.L. Brakora, Y. Ra, R.D. Reitz, J. McFarlane, C.S. Daw, Development and validation of a reduced reaction mechanism for biodiesel-fueled engine simulations, *SAE International Journal of Fuels and Lubricants*, **1** (2009) pp.675-702.
- [28] T. Vaughn, M. Hammill, M.Harris, A.J. Marchese, Ignition delay of bio-ester fuel droplets. SAE Paper No.2006-01-3302; 2006.
- [29] S. Som, D.E. Longman, Numerical study comparing the combustion and emission characteristics of biodiesel to petrodiesel, *Energy Fuels*, **25** (2011) pp.1373-1386.
- [30] S.M. Sarathy, M.J. Thomson, W.J. Pitz, T. Lu, An experimental and kinetic modeling study of methyl decanoate combustion, *Proc. Combust. Inst.*, **33** (2011) pp.399-405.
- [31] K. Seshadri, T.F. Lu, O. Herbinet, S.B. Humer, U. Niemann, W.J. Pitz, R. Seiser, C.K. Law, Experimental and kinetic modeling study of extinction and ignition of methyl decanoate in laminar non-premixed flows, *Proc. Combust. Inst.*, **32** (2009) pp.1067-1074.
- [32] Z. Luo, T. Lu, M.J. Maciaszek, S. Som, D.E. Longman, A reduced mechanism for high temperature oxidation of biodiesel surrogates, *Energy Fuels*, **24** (2010) pp.6283–6293.

- [33] J.L. Brakora, Y. Ra, R.D. Reitz, Combustion model for biodiesel-fueled engine simulations using realistic chemistry and physical properties, *SAE International Journal of Engines*, **4** (2011) pp.931-947.
- [34] M.Mehl, W.J. Pitz, C.K. Westbrook, H.J. Curran, Kinetic modeling of gasoline surrogate components and mixtures under engine conditions *Proc. Combust. Inst.*, **33** (2011) pp.193-200.
- [35] S.M. Sarathy, C.K. Westbrook, M. Mehl, W.J. Pitz, C. Togbe, P. Dagaut, H. Wang, M.A. Oehlschlaeger, U. Niemann, K. Seshadri, P.S. Veloo, C. Ji, F.N. Egolfopoulos, T. Lu, Comprehensive chemical kinetic modeling of the oxidation of 2-methylalkanes from C7 to C20 *Combust. Flame*, in press (2011).
- [36] P.K. Senecal, E. Pomraning, K.J. Richards, T.E. Briggs, C.Y. Choi, R.M. McDavid, M.A. Patterson, Multi-dimensional modeling of direct-injection diesel spray liquid length and flame lift-off length using CFD and parallel detailed chemistry. SAE Paper No.2003-01-1043; 2003.
- [37] P.K. Senecal, K.J. Richards, E. Pomraning, T. Yang, M.Z. Dai, R.M. McDavid, M.A. Patterson, S. Hou, T. Shethaji, A new parallel cut-cell cartesian CFD code for rapid grid generation applied to in-cylinder diesel engine simulations. SAE Paper No.2007-01-1059; 2007.
- [38] S.Som, Development and validation of spray models for investigating diesel engine combustion and emissions. Ph.D Thesis, University of Illinois at Chicago; 2009.
- [39] S. Som, D.E. Longman, A.I. Ramirez, S.K. Aggarwal, A comparison of injector flow and spray characteristics of biodiesel with petrodiesel, *Fuel*, **89** (2010) pp.4014-4024.
- [40] S.Som, A.I. Ramirez, D.E.Longman, S.K.Aggarwal, Effect of nozzle orifice geometry on spray, combustion, and emission characteristics under diesel engine conditions, *Fuel*, **90** (2011) pp.1267-1276.
- [41] R.D. Reitz, Modeling atomization process in high pressure vaporizing sprays, *Atomization and Spray Technology*, **3** (1987) pp.309-337.
- [42] M.A. Patterson, R.D. Reitz, Modeling the effects of fuel spray characteristics on diesel engine combustion and emission. SAE Paper No.980131; 1998.
- [43] D.P. Schmidt, C.J. Rutland, A new droplet collision algorithm, *J. Comput. Phys.*, **164** (2000) pp.62-80.
- [44] S.L. Post, J. Abraham, Modeling the outcome of drop-drop collisions in Diesel sprays, *Int. J. Multiphase Flow*, **28** (2002) pp.997-1019.
- [45] A.B. Liu, D.K. Mather, R.D. Reitz, Modeling the effects of drop drag and breakup on fuel sprays. SAE Paper No.930072; 1993.
- [46] Engine Combustion Network Website. <http://www.sandia.gov/ecn/>.
- [47] Y. Ra, R.D. Reitz, J. McFalan, C.S. Law, Effects of fuel physical properties on diesel engine combustion using diesel and bio-diesel fuels. SAE Paper No.2008-01-1379; 2008.
- [48] J. Herzler, L. Jerig, P. Roth, Shock tube study of the ignition of lean n-heptane/air mixtures at intermediate temperatures and high pressures, *Proc. Combust. Inst.*, **30** (2005) pp.1147-1153.
- [49] P. Dievart, S. Dooley, S.H. Won, F.L. Dryer, Y. Ju, Kinetic studies and experimental assessment of high temperature oxidation of methyl decanoate, 7th US National Combustion Meeting, Atlanta, GA, 2011.
- [50] P. Dagaut, S. Gail, M. Sahasrabudhe, Rapeseed oil methyl ester oxidation over extended ranges of pressure, temperature, and equivalence ratio: Experimental and modeling kinetic study, *Proc. Combust. Inst.*, **31** (2007) pp.2955-2961.
- [51] Y.L. Wang, Q. Feng, F.N. Egolfopoulos, T.T. Tsotsis, Studies of C4-C10 methyl ester flames, *Combust. Flame*, **158** (2011) pp.1507-1519.

- [52] S. Sarathy, M. Thomson, W. Pitz, T. Lu, An experimental and kinetic modeling study of methyl decanoate combustion, *Proc. Combust. Inst.*, **33** (2010), pp.399-405.
- [53] D.L. Siebers, B.Higgins, Flame lift-off on direct-injection diesel sprays under quiescent conditions. SAE Paper No.2001-01-0530; 2001.
- [54] B.Higgins, D.L. Siebers, Measurement of the flame lift-off location on DI diesel sprays using OH chemiluminescence. SAE Paper No.2001-01-0918; 2001.
- [55] S.Som, S.K.Aggarwal, Effects of primary breakup modeling on spray and combustion characteristics of compression ignition engines, *Combust. Flame*, **157** (2010) pp.1179-1193.
- [56] J.G. Nerva, C.L. Genzale, J.M.G. Oliver, L.M. Pickett, Sandia National Laboratories, Livermore, CA. *Personal communication*, 2010.
- [57] J.D. Naber, D.L. Siebers, Effects of gas density and vaporization on penetration and dispersion of diesel sprays. SAE Paper No.960034; 1996.
- [58] G. Vishwanathan, R.D. Reitz, Development of a practical soot modeling approach and its application to low-temperature diesel combustion. *Combust. Sci. Technol.*, **182** (2010) pp.1050-1082.

### Figure Captions

**Figure 1:** The temperature profiles of auto-ignition to demonstrate the effect of error cancellation.

**Figure 2:** Grid generated in CONVERGE at 0.4 ms ASI for combustng sprays described in Table 1.

**Figure 3:** Comparison of the 89-species skeletal mechanism with the detailed mechanism for biodiesel-air, a) ignition delays, and b) extinction temperature profiles in PSR.

**Figure 4:** Comparison of simulated and measured ignition delay times as a function of the initial temperature for n-heptane/air mixture at pressure of 50 bar and equivalence ratio of 0.4. The measurement data were obtained from Ref. [48]. The calculation was performed with the detailed and 89-species skeletal mechanisms, respectively.

**Figure 5:** Comparison of simulated and measured ignition delay times as a function of the initial temperature for MD-O<sub>2</sub>-Ar mixture at pressure of 7atm, equivalence ratio of 0.09 and fuel mole fraction of 1005 ppm. The measurement data were obtained from Ref. [49]. The calculation was performed with the detailed and 89-species skeletal mechanisms, respectively.

**Figure 6:** Species concentrations in JSR as a function of temperature for RME at pressure of 10 atm and residence time of 1s. Symbols: experimental data [50], solid lines: values calculated with the detailed mechanism, dash lines: values calculated with the 89-species skeletal mechanism.

**Figure 7:** Laminar flame speed as a function of the equivalence ratio for MD-air mixture at atmospheric pressure and initial temperature of 403K. Symbols: experimental measurements [51], lines: calculated values with the 89-species skeletal mechanism.

**Figure 8:** Species profiles computed with the 89-species skeletal mechanism (lines) compared with experimental measurements (symbols) by Sarathy et al. [52], for opposed-flow flames under atmospheric pressure.

**Figure 9:** Measured [56] and predicted liquid spray penetration and vapor penetration vs. time for biodiesel fuel at an ambient temperature of 900K.

**Figure 10:** Validation of flame lift-off length against the OH-chemiluminescence data from Ref. [56] at 900K and 1000K. The average equivalence ratio at flame lift-off location is also indicated.

**Figure 11: Comparison of OH mole-fraction contours from simulations against the OH-chemiluminescence data from Ref.[56], at different instances during the combustion process at an ambient temperature of 1000K.**

**Figure 12: Comparison of soot mole-fraction contours from simulations against the soot data using LII from Ref. [56] at different instances during the combustion process at an ambient temperature of 1000K.**

**Figure 13: Comparison of soot mole-fraction contours from simulations against the soot data using LII from Ref. [56] at different instances during the combustion process at an ambient temperature of 1000K.**

**Table 1:**  
Test conditions for combustion experiments at Sandia National Laboratories [56].

Parameter	Quantity
Injection System	Bosch Common Rail
Nozzle Description	Single-hole, mini-sac
Duration of Injection [ms]	7.5
Orifice Diameter [μm]	90
Injection Pressure [Bar]	1400
Fill Gas Composition (mole-fraction)	N <sub>2</sub> =0.7515, O <sub>2</sub> =0.15, CO <sub>2</sub> =0.0622, H <sub>2</sub> O=0.0363
Chamber Density [kg/m <sup>3</sup> ]	22.8
Chamber Temperature [K]	900, 1000
Fuel Density @ 40°C [kg/m <sup>3</sup> ]	877 (Soy-biodiesel)
Fuel Injection Temperature [K]	373

Table 2:

Validation of simulation results for ignition delay, flame lift-off length, and equivalence ratio at lift-off location against data from Sandia National Laboratory [56] at 900K and 1000K.

	Ignition Delay	Lift-off length	Equivalence Ratio		
	(ms)	(mm)			
Sandia Data	0.683	26.18	1.35	}	T = 900 K
Uconn-89 Mechanism	0.741	30.17	1.21		
Sandia Data	0.396	17.27	2.08	}	T = 1000 K
Uconn-89 Mechanism	0.391	18.76	2.04		

Figure1

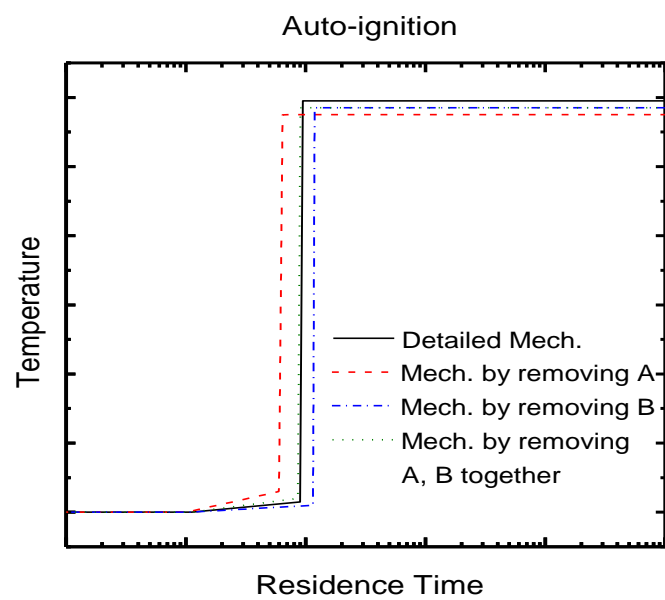


Figure2

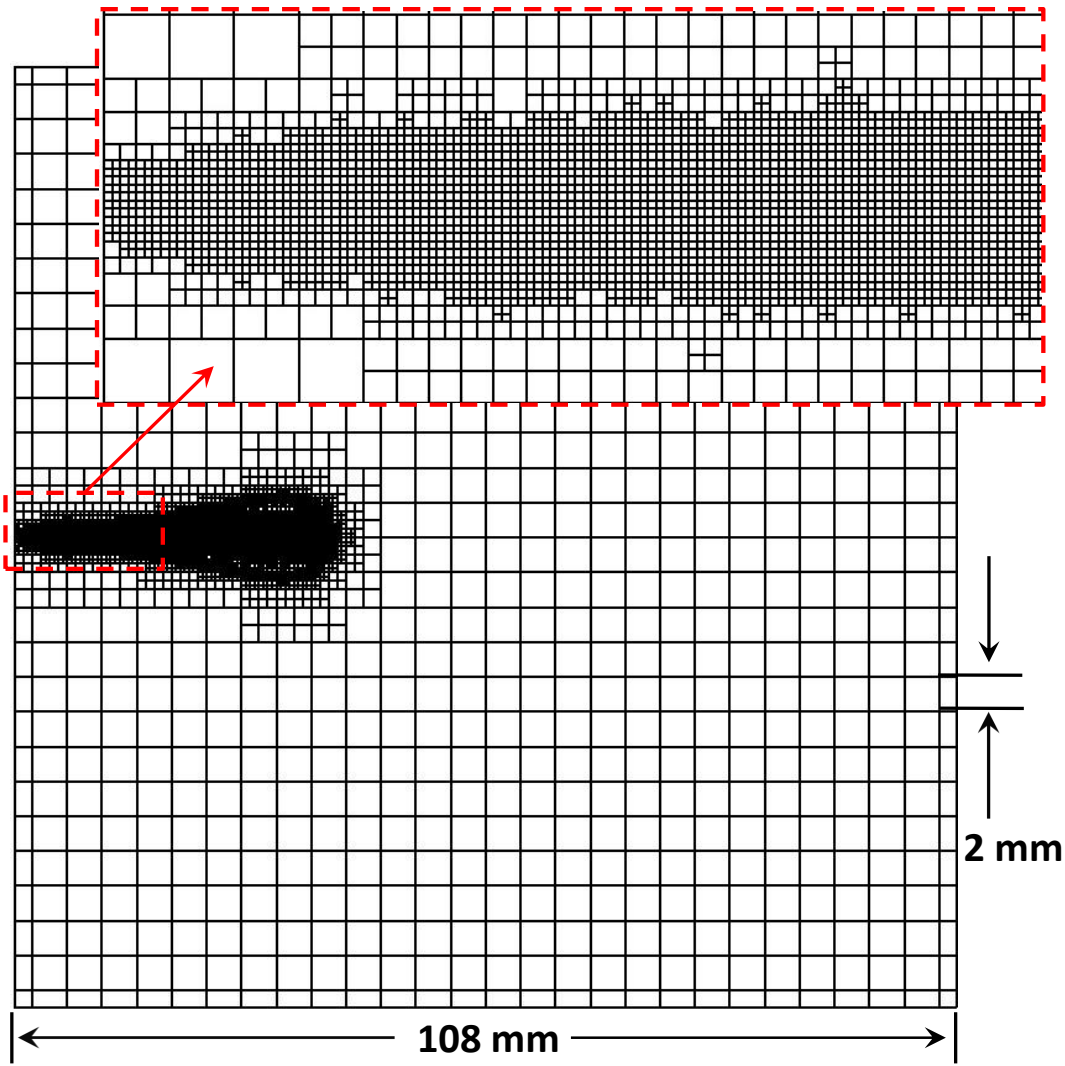


Figure3

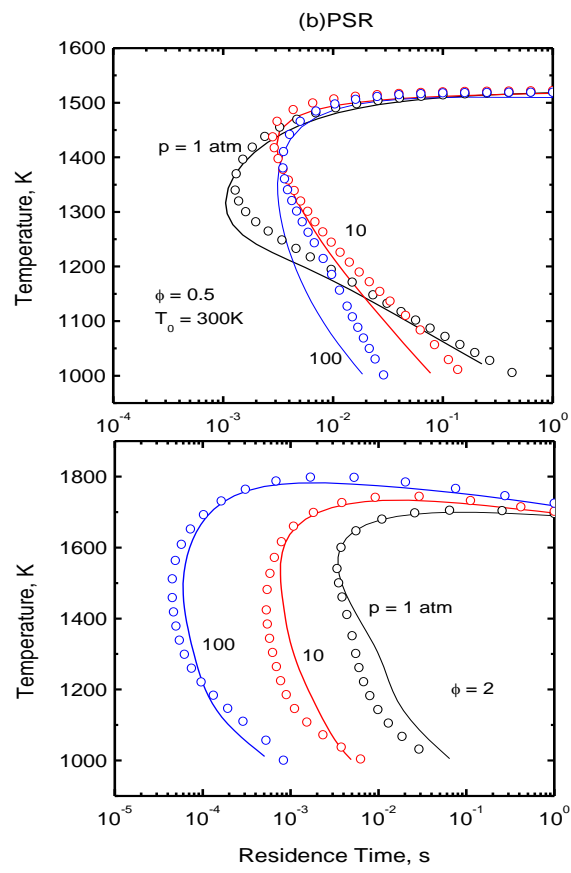
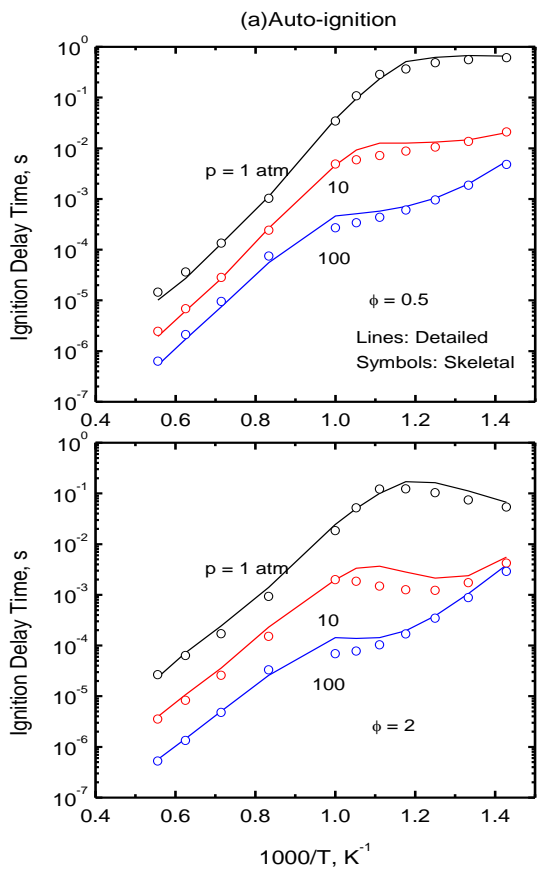


Figure4

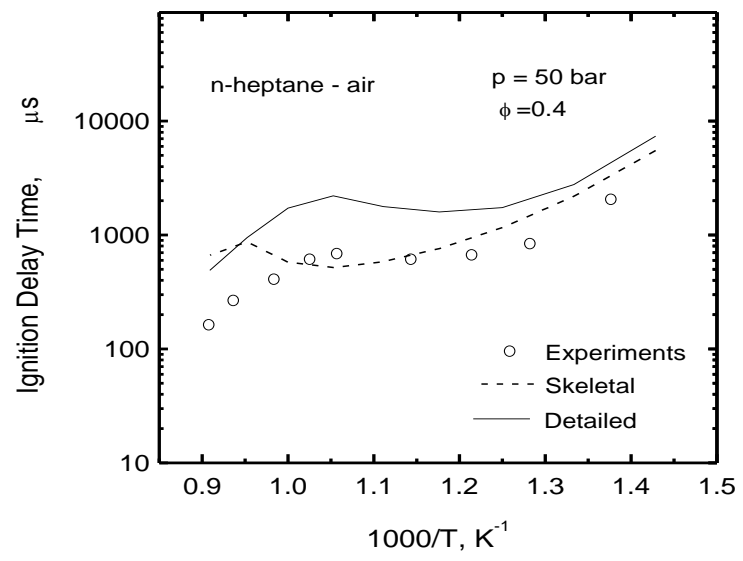


Figure5

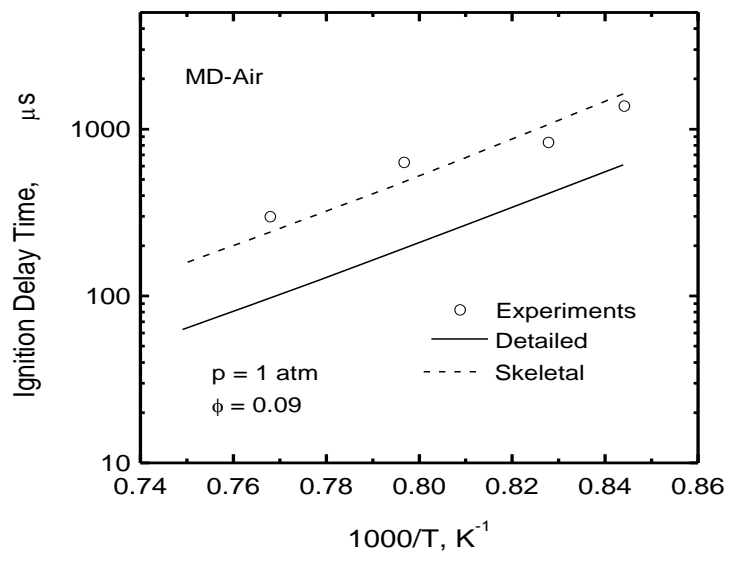


Figure6

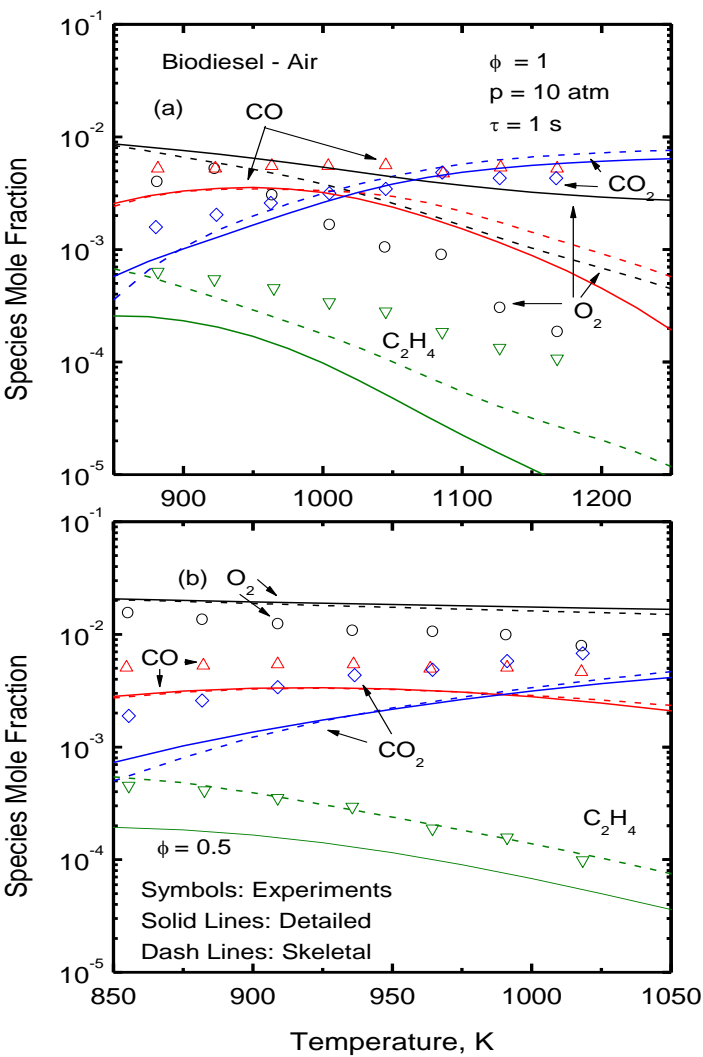


Figure7

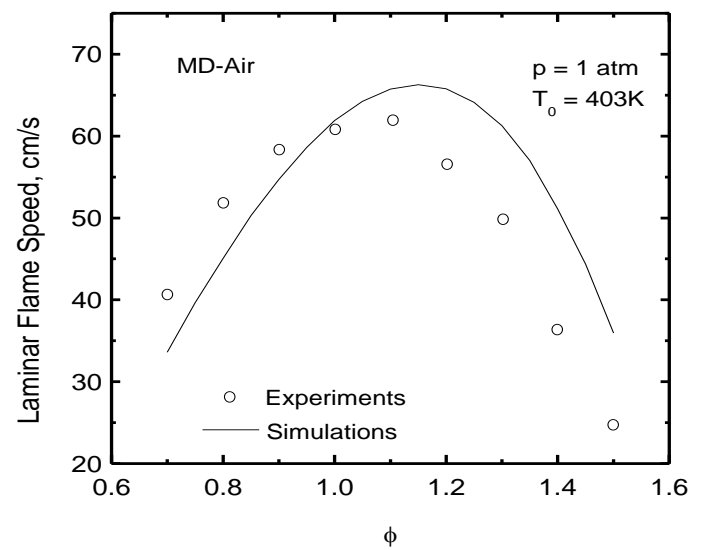


Figure8

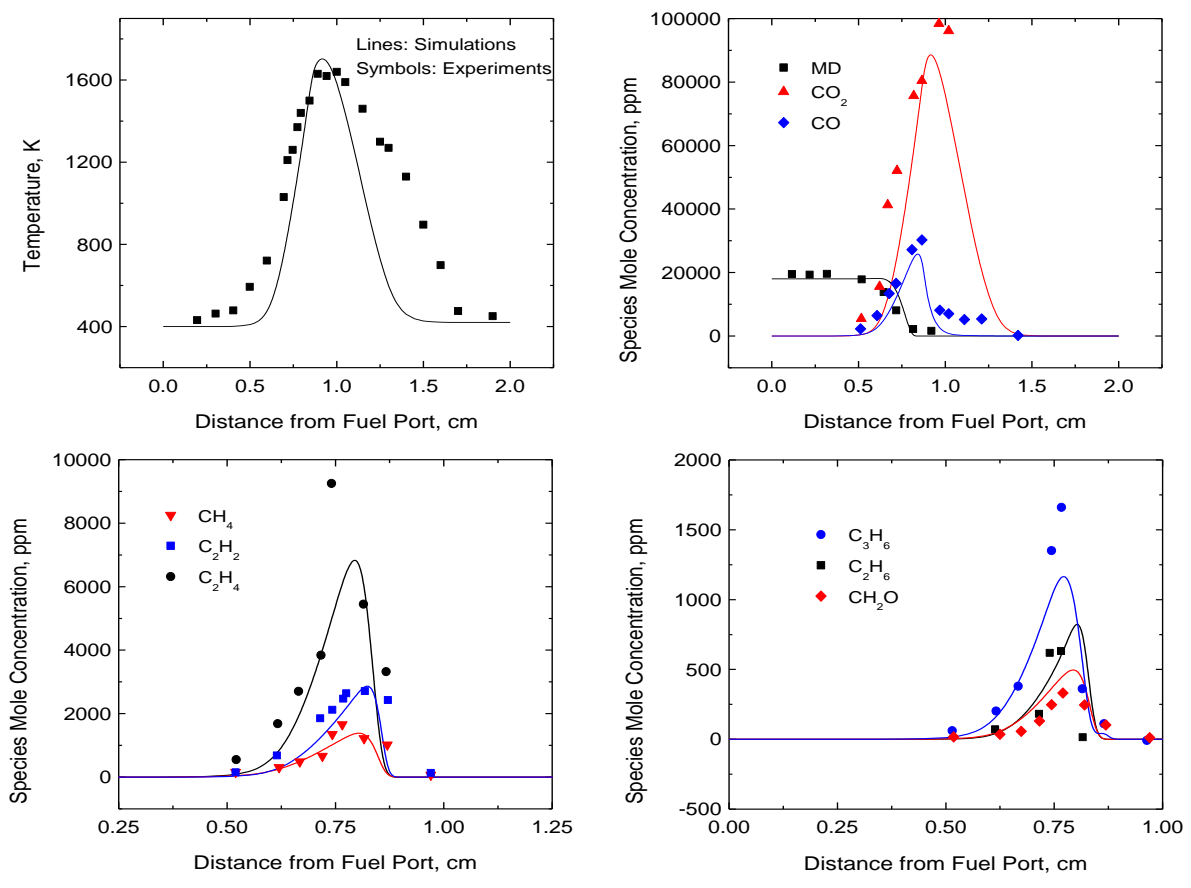


Figure9

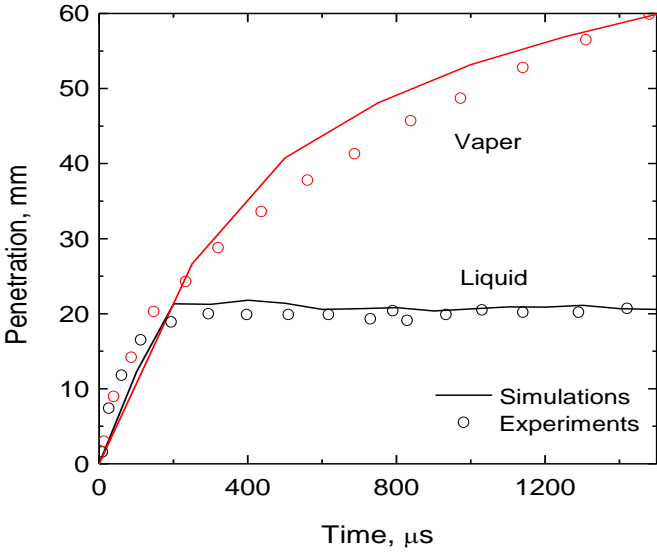


Figure10

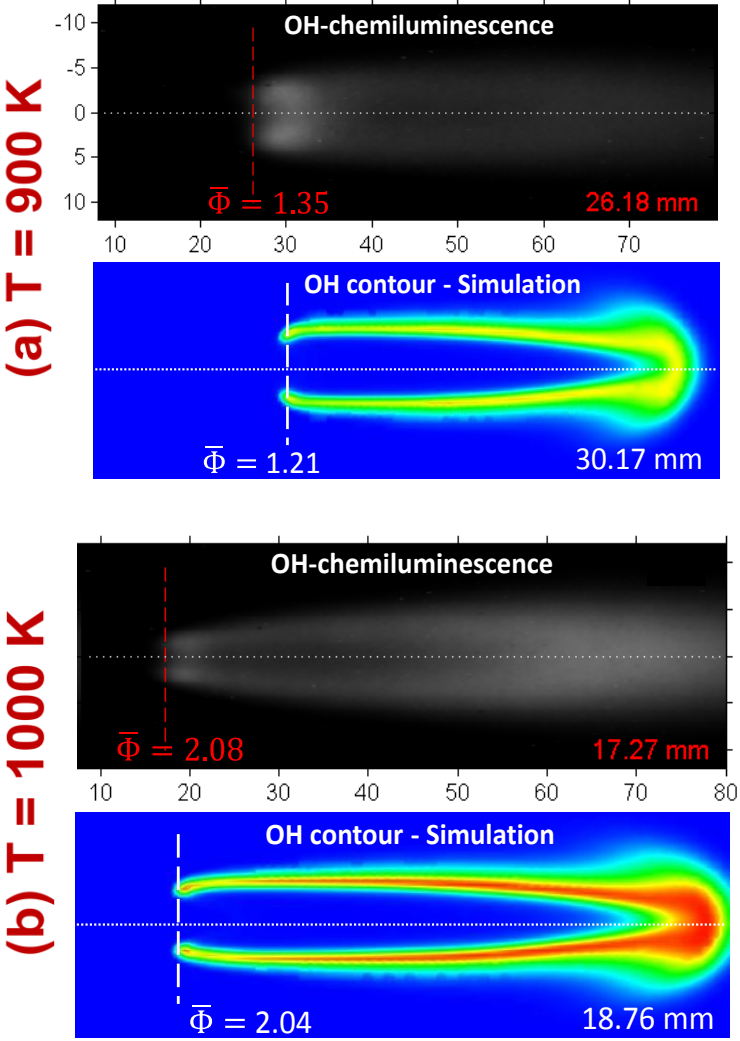


Figure11

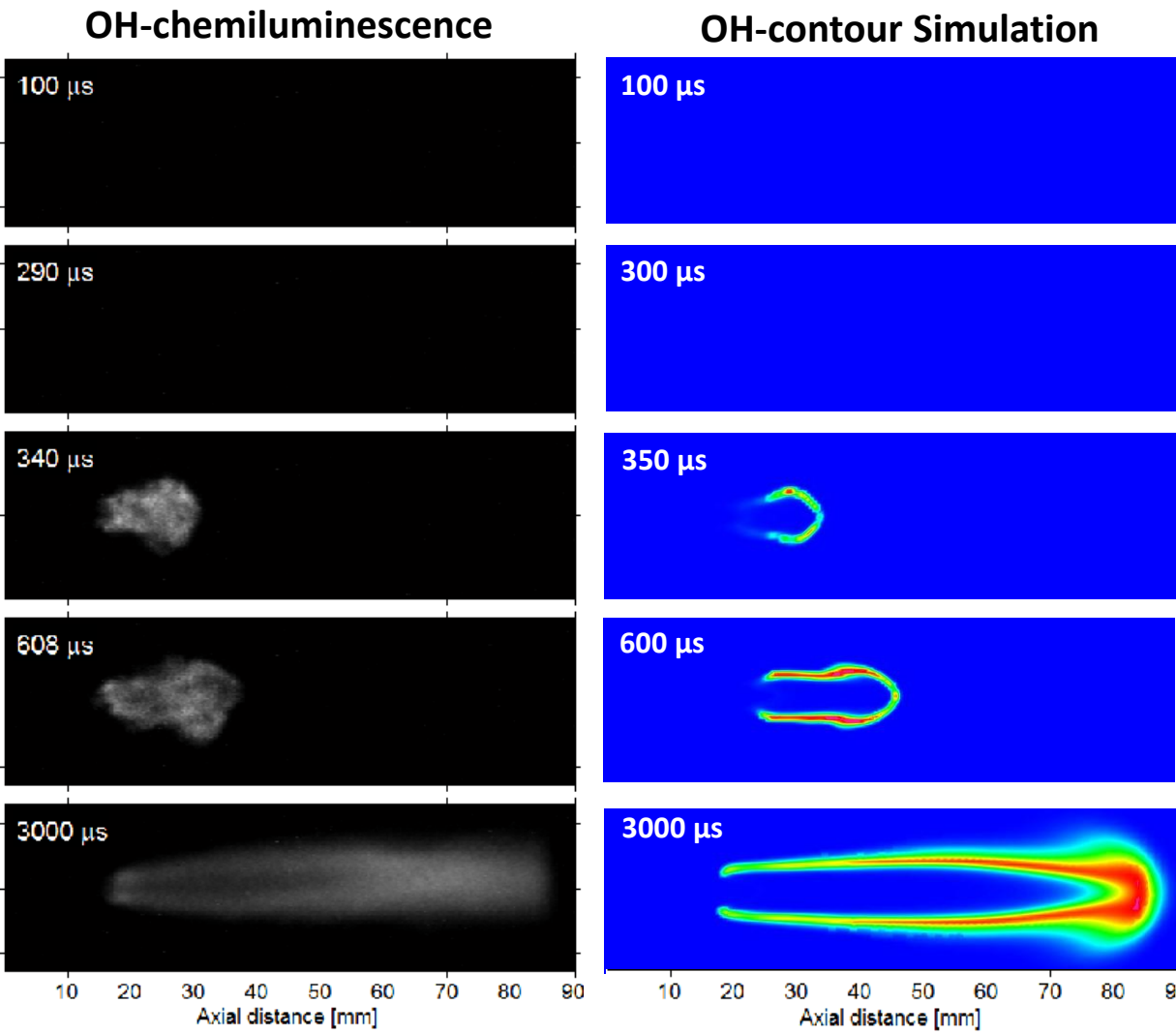


Figure12

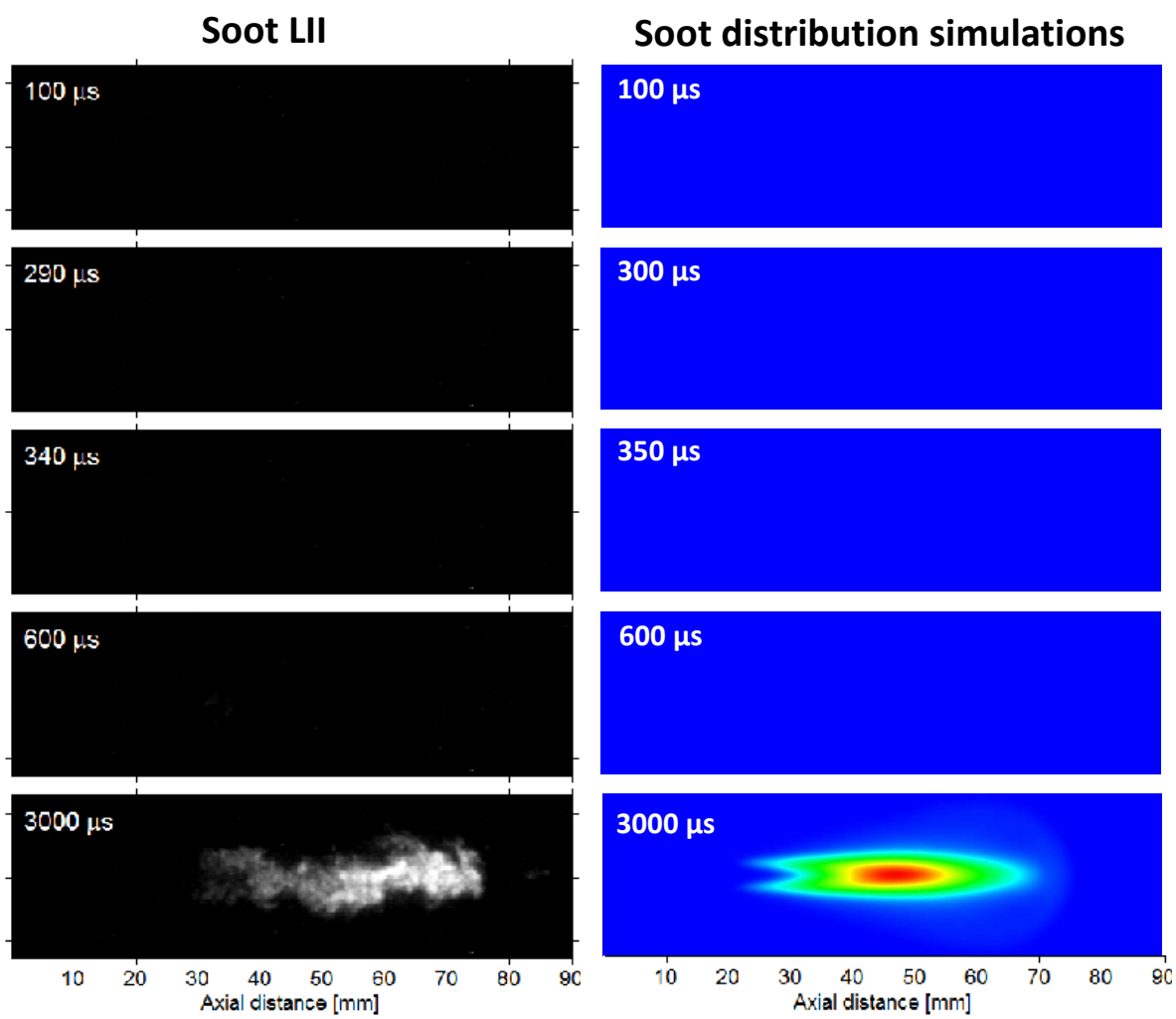


Figure13

